ACS APPLIED BIO MATERIALS

Article

Magnetic nanoplatforms for in situ modification of macromolecules: synthesis, characterization and photoinactivating power of cationic nanoiman-porphyrin conjugates

Ana Coral Scanone, Natalia Soledad Gsponer, Maria Gabriela Alvarez, Daniel Alejandro Heredia, Andrés M. Durantini, and Edgardo Néstor Durantini

ACS Appl. Bio Mater., **Just Accepted Manuscript** • DOI: 10.1021/acsabm.0c00625 • Publication Date (Web): 06 Aug 2020

Magnetic nanoplatforms for *in situ* modification of macromolecules: synthesis, characterization and photoinactivating power of cationic nanoiman-porphyrin conjugates

Ana C. Scanone, Natalia S. Gsponer, María G. Alvarez, Daniel A. Heredia, Andrés M. Durantini and Edgardo N. Durantini*

IDAS-CONICET, Departamento de Química, Facultad de Ciencias Exactas, Físico-Químicas y Naturales, Universidad Nacional de Río Cuarto, Ruta Nacional 36 Km 601, X5804BYA Río Cuarto, Córdoba, Argentina.

* Corresponding author.

E-mail address: edurantini@exa.unrc.edu.ar (E.N. Durantini)

ABSTRACT

Nanoplatform concept was developed to synthesized accessible photoactive magnetic nanoparticles (MNPs) of Fe_3O_4 coated with silica. This approach was based on the covalent binding of 5,10,15,20-tetrakis(pentafluorophenyl)porphyrin ($TPPF_{20}$) to aminopropyl-grafted MNPs by nucleophilic aromatic substitution reaction (S_NAr) to obtain conjugate MNP-P1. After *in situ* modification, the remaining pentafluorophenyl groups of $TPPF_{20}$ attached to MNPs were substituted by dimethylaminoethoxy groups to form MNP-P2. The basic amine group of these conjugates can be protonated in aqueous media. In addition, MNP-P1 and MNP-P2 were intrinsically charged to produce cationic conjugates MNP^+-P1 and MNP^+-$P2^+$ by methylation. All of them were easily purified by magnetic decantation in high yields. The average size of the MNPs was ~15 nm and the main difference between these conjugates was the greater coating with positive charges of MNP^+-$P2^+$, as showed by the zeta potential values. Absorption spectra exhibited the Soret and Q bands characteristic of $TPPF_{20}$ linked to MNPs. Furthermore, these conjugates showed red fluorescence emission of porphyrin with quantum yields of 0.011-0.036. The photodynamic effect sensitized by the conjugates indicated the efficient formation of singlet molecular oxygen in different media, reaching quantum yields values of 0.17-0.34 in *N*,*N*-dimethylformamide. The photodynamic activity of the conjugates was evaluated to inactivate the Gram-positive bacteria *Staphylococcus aureus*, the Gram-negative bacteria *Escherichia coli* and the yeast *Candida albicans*. The modified cationic MNP^+-$P2^+$ was the most effective conjugate for photodynamic inactivation (PDI) of microorganisms. Binding of this conjugate to bacteria and photoinactivation capability was checked by means of fluorescence microscopy. Also, sustainable use by recycling was determined after three PDI treatments. Therefore, this methodology is a suitable scaffold for the *in situ* modification of conjugates and in particular, MNP^+-$P2^+$ represents a useful photodynamic active material to eradicate microorganisms.

KEYWORD: magnetic nanoparticles, porphyrin, nanoplatform, photodynamic inactivation, antimicrobial.

1. INTRODUCTION

Magnetic nanoparticles (MNPs) are suitable to be decorated with different functional group and due to its magnetic properties, they can be visualized and guided in water and organic solvents by means of an external magnetic field.[1] This effect allowed to exploit different pathways and applications of MNPs, from cellular targeting and hyperthermia therapy to the petroleum industry for emulsion separations.[2-4] In particular, an interesting potential use of photosensitizer conjugated to MNPs involve the photodynamic inactivation (PDI) of microorganisms.[5,6] This procedure is based on the addition of a photosensitizer to the medium contaminated with pathogenic microorganisms. Next, irradiation with visible light mainly leads to the formation of reactive oxygen species (ROS), which cause lethal damage to the microbial cells.[7] In this sense, nanomagnet-porphyrin hybrids have been studied as efficient photosensitizers to inactivate bacteria and phages.[8,9] Also, porphyrin conjugated to MNPs has been proposed to control microbial proliferation by PDI.[10]

Many of these MNPs-conjugated photosensitizers were formed using AB_3-porphyrins. These asymmetrically substituted tetrapyrrole macrocycles contain three identical molecular structures B and one different A at the *meso*-position. In those cases, the structure A bears a functional group that can be used to link the porphyrin with other molecules, while B contain substituents that allow changing the polarity and interaction with the media.[11] These porphyrins can be synthesized by a binary mixed aldehyde and pyrrole condensation. The purification requires slow chromatographic separation with very poor yields (<3%).[12] Also, AB_3-porphyrins can be obtained by the condensation of a dipyrromethane with a binary mixture of aldehydes. This approach involves two steps of synthesis and purification, using flash chromatography a large amount of organic solvents, with yields <15%.[11,13] However, there are no reports that indicate the use of MNPs as nanoplatform for the *in situ* modification of photosensitizers. Therefore, a porphyrin with a sophisticated synthetic procedure and low reaction yield could be easily modified starting from a tetrapyrrole macrocycle covalently linked to MNPs. After each synthetic step, a desired macrocycle attached to MNPs can be isolated from

byproducts by washing using the magnetic decantation technique. This purification method also avoids the use of excessive amounts of organic solvents that are usually required in organic synthesis.

Considering our interest in developing accessible photoactive MNPs to inactivate microorganisms, here we report this new nanoplatform concept to facilitate the synthesis of four conjugates using 5,10,15,20-tetrakis(pentafluorophenyl)porphyrin ($TPPF_{20}$) as a structurally modifiable photosensitizer. This A_4-porphyrin is commercially accessible or can be easily synthesized with good yields.[14,15] This porphyrin is a suitable and versatile building block for the construction of *meso*-substituted tetrapyrrolic macrocycles through the nucleophilic aromatic substitution reaction (S_NAr).[16] After *in situ* modification different conjugates were obtained, two of them (MNP-P1 and MNP-P2) do not present net intrinsic charges, while the other two (MNP^+-P1 and MNP^+-$P2^+$) are substituted with cationic groups (Figure 1). The absorption and fluorescent spectroscopic characteristics of the MNPs-conjugated porphyrins were assessed in different media. Moreover, their photodynamic properties were studied in the presence of different photooxidizable substrates. The photodynamic activity of the conjugates was investigated to inactivate the Gram-positive bacteria *Staphylococcus aureus*, the Gram-negative bacteria *Escherichia coli* and the yeast *Candida albicans*. These bacteria are representative of microorganisms responsible for numerous hospital-acquired infections and water-related diseases.[17,18] Furthermore, invasive fungal infections are a major cause of morbidity and mortality in hospitalized patients.[19] Therefore, this study was also focused on the ability to applicate these MNPs-conjugated porphyrins to photoinactivate these pathogens.

2. EXPERIMENTAL SECTION

2.1. Synthesis of MNPs and conjugates

The conjugates of MNPs with $TPPF_{20}$ were synthesized following the procedures schematically shown in Figure S1. $TPPF_{20}$ was synthesized as previously reported.[15]

2.1.1. Synthesis of $MNPSiNH_2$

The synthesis of $MNPSiNH_2$ was done as previously described.[10,20] Briefly, MNPs of iron oxide (Fe_3O_4) were synthesized from $FeCl_2$ and $FeCl_3$ using the coprecipitation technique, followed by treatment with sodium metasilicate (Na_2SiO_3) to obtain MNPs coated with silica (MNPSi, average size 10 ± 2 nm). Finally, (3-aminopropyl)triethoxysilane (APTS) was added to form MNPs functionalized with amine groups ($MNPSiNH_2$, average size 11 ± 2 nm).

2.1.2. Synthesis of MNP-P1

The covalent binding of $TPPF_{20}$ to $MNPSiNH_2$ was performed as described for pentafluorophenyl derivatives with amine groups with same modifications.[21,22] From a suspension of $MNPSiNH_2$ in water (84 mL, 4 mg $MNPSiNH_2$/mL) the solvent was eliminated by magnetic decantation. Then, the $MNPSiNH_2$ were washed with freshly distilled *N,N*-dimethylformamide (DMF) and resuspended in 10 mL of the same solvent. This suspension was mixed with a solution of $TPPF_{20}$ (2 mL, 20 mM) in DMF. The reaction mixture was stirred at room temperature for 48 h. The progress of the reaction was followed by TLC analysis (silica gel; *n*-hexane / chloroform 3:2) of the supernatant in the mixture, which showed the consumption of $TPPF_{20}$ ($R_f = 0.45$) due to the formation of the conjugate with the MNPs. The reaction mixture was sonicated for 5 min, then placed on a neodymium magnet for 5 min to produce magnetic decantation of the MNPs. The supernatant was discarded to remove non-magnetic materials. MNPs were resuspended in 10 mL DMF, sonicated for 5 min, kept for 15 min at room temperature, recollected by magnetic decantation and the solvent was discarded. This washing process was repeated several times until the presence of impurities were not detected in the supernatant by UV-visible absorption spectroscopy in the range of 250-800 nm. This first washing process was followed by a similar procedure but using acetone and methanol. In each washing step, 10 mL of solvent were used. The amount of $TPPF_{20}$ attached to the MNPs was calculated by subtracting the amount of recovered $TPPF_{20}$ in the combined washing solvents

(measured by UV-visible absorption spectroscopy) to the initial amount of $TPPF_{20}$ used. The MNP-P1 conjugate obtained was resuspended in 84 mL water.

2.1.3. Synthesis of MNP^{+}-P1 and $MNPSiN^{+}(CH_3)_3$

The formation of cationic groups was carried out with a large excess of CH_3I.[8] The water in the MNP-P1 suspension (21 mL, 4 mg MNP-P1/mL) was discarded by magnetic decantation. After successive washing with DMF, the MNPs were resuspended in 21 mL of the same solvent and 2 mL of CH_3I were added. The reaction mixture was stirred 72 h at 40 °C. After this reaction time, the new MNP^{+}-P1 were washed with DMF by magnetic decantation as described in 2.1.2 and resuspended in 21 mL water. The same procedure was used to obtain $MNPSiN^{+}(CH_3)_3$.

2.1.4. Synthesis of MNP-P2

The derivatization of $TPPF_{20}$ attached to MNP-P1 was achieved similarly to the reactions of pentafluorophenyl porphyrinoids with alcohols.[23] After washing MNP-P1 (42 mL, 4 mg MNP-P1/mL) by magnetic decantation with freshly distilled tetrahydrofuran (THF), the conjugate was resuspended in THF (10 mL). Then, 2-(*N*,*N*-dimethylamino)ethanol (DAE, 80 μmol), anhydrous potassium hydroxide (KOH, 64 μmol) and tetrabutylammonium bromide (TBAB, 100 μL) were added. The reaction mixture was continuosly stirred at room temperature for 12 h. The MNP-P2 were purified whashing with THF and water by magnetic decantation following the methodology detailed in 2.1.2 and the conjugated was resuspended in 42 mL water.

2.1.5. Synthesis of MNP^{+}-$P2^{+}$

An aliquot of MNP-P2 (21 mL) was methylated with CH_3I following the procedure described above for the synthesis of MNP^{+}-P1. After washing with DMF by magnetic decantation as indicated in 2.1.2, MNP^{+}-$P2^{+}$ was resuspended in 21 mL water.

2.2. Preparation of samples of the MNPs conjugates

After the synthesis of each conjugate, aliquots that were used as a stock suspension in the different studies were separated (Figure S1). The recovery of the conjugates after each process was calculated by weighing. Stock solutions were prepared at the same concentration for all conjugates, which was 4 mg MNPs/mL containing 10 nmol porphyrin/mg MNPs. Before each experiment, the solutions were sonicated for 5 min to disaggregate the MNPs.

2.3. Morphology of MNPs and zeta potential determinations

The morphology and size of the MNPs were examined by transmission electron microscopy (TEM). A drop of each suspension of MNPs conjugate was placed on a formvar-coated copper grid and the solvent was evaporated under reduced pressure. The zeta potential (ζ) determinations were performed using aqueous dispersions of the different MNPs conjugates. The measurements were carried out in 1 mg/mL dispersions of the corresponding samples, ultrasonically dispersed for 5 min. Electrophoretic mobilities were converted to ζ using the Smoluchowski equation.[24]

2.4. Spectroscopic studies

UV-visible absorption and fluorescence spectra of the different conjugates (concentration between 1-2 μM in immobilized porphyrin) were recorded as reported.[20] An excitation wavelength of 428 nm was used to acquire the emission spectra. 5,10,15,20-Tetrakis(4-sulfonatophenyl)porphyrin ($TPPS^{4-}$) was used as a reference (Φ_F = 0.080) to determine the fluorescence quantum yield (Φ_F) of each MNPs conjugates in water.[25] All spectral measurements were performed at room temperature using a quartz cell of 1 cm path length. The absorbances of the conjugates and $TPPS^{4-}$ (<0.05) were matched at the excitation wavelength. The areas under the emission spectra were integrated and compared in the 600-800 nm range.

2.5. Steady state photolysis of substrates

Photooxidation of tetrasodium 2,2'-(anthracene-9,10-diyl)bis(methylmalonate) (ABMM) and 9,10-dimethylantracene (DMA) were performed in aqueous media and DMF, respectivaly.[10,20] Samples of anthracene derivative (35 μM) in the presence of MNPs conjugates (3 μM of immobilized porphyrin) were irradiated with light (455-800 nm) in 1 cm path length quartz cells (2 mL). The photooxidation rate of both substrates were studied by following the decrease of the absorbance at 378 nm for DMA and 379 nm for ABMM. The observed rate constants (k_{obs}) and quantum yields of $O_2(^1\Delta_g)$ production (Φ_Δ) were calculated as previously reported, using $TPPS^{4-}$ was used as a reference ($\Phi_\Delta = 0.71$).[26,27]

2.6. Strains and cultures of microorganism

The microbial strains were *S. aureus* ATCC 25923, *E. coli* EC7 and *C. albicans* PC31 that were previously characterized and identified.[28] Cultivation of microorganisms and handling of cells to obtain ~10^8 colony forming units (CFU)/mL for bacteria and ~10^6 CFU/mL for yeast in phosphate-buffered saline (PBS, pH = 7.4) were achieved as reported.[10] Viable microbial cells were quantified after serial dilutions 10-fold in PBS by the spread plate technique after an incubation of 24 h for bacteria or 48 h for yeast at 37 °C in the dark.

2.7. Photoinactivation of microorganisms

Cell suspensions (1.9 mL) of *E. coli* (10^8 CFU/mL) and *S. aureus* (10^8 CFU/mL) and *C. albicans (*10^6 CFU/mL) in PBS were incubated with 0.1 mL MNPs conjugate in Pyrex culture tubes (13x100 mm) for 30 min in the dark at 37 °C. That mean the addition of 0.4 mg MNPs conjugate in a final volume of 2 mL (0.2 mg MNPs conjugate/mL, 2 μM immobilized $TPPF_{20}$). The same conditions were used with $MNPSiN^+(CH_3)_3$. Subsequently, 200 μL of the cell suspensions were transferred to 96-well microtiter plates. The cultures were exposed to visible light (90 mW/cm^2) for different irradiation periods (5, 15 and 30 min, which match the light fluences of 27, 81 and 162 J/cm^2, respectively). Description of the light source was previously reported.[29] After each irradiation

time, a 100 µl aliquot of wells was taken to perform 10-fold serial dilutions in PBS of the bacterial cells. Different wells were used for each irradiation period. Viable cells were quantified as mentioned in section 2.6. Three values were obtained per each condition and each experiment was repeated separately three times. For recycling experiments, MNPs conjugates were recovered by magnetic decantation after PDI treatment and resuspended in a new cell suspension. An average time of 5 min was used to collect the MNP by the application of the external magnetic field. The cultures were kept in the dark for 30 min and irradiated again to complete the cycle.[10] The unpaired *t*-test was used to obtain the significance of differences between experiments. Differences between means were tested for significance by one-way ANOVA. Results were statistically significant with a confidence level of 95% ($p < 0.05$). Data were denoted as the mean ± standard deviation of each experiment. Controls were performed with cultures of microorganisms in the dark, with and without conjugates and irradiated cells in the absence of conjugates.

2.8. Bioimaging and PDI by fluorescence microscopy

Fluorescence microscopy investigations were carried out using the methodology previously reported with same modifications.[20,30] Bacterial suspension (100 µL) was incubated in a chamber composed of a polymeric cylinder glue to a coverslip for 30 min. This procedure was used to allow cells to attach to the glass surface. Unbound bacteria were removed by washing with PBS. Bioimaging experiments were performed addicting 200 µL MNP^{+}-$P2^{+}$ (0.8 mg MNPs) to attached cells on glass surface of a chamber. Cells were incubated for 30 min in dark, the chamber was rinsed to eliminate MNPs the chamber was rinsed with PBS to remove the MNPs that were not bound to the cells and filled with 500 µL PBS. After PDI treatments, the cell viability was determined with propidium iodide (PI). Fluorescence images PI were performed using an emission band pass filter (645/75). The fluorescence emitted from the MNP^{+}-$P2^{+}$ or PI was collected by the same objective and captured in a CMOS camera. Phase contrast images were also attained to verify bacterial presence in the sample chamber.

3. RESULTS AND DISCUSSION

3.1. Design of the new conjugates nanomagnet-porphyrin

The synthesis of MNPs conjugates with $TPPF_{20}$ are summarized in Figure 1. This is an idealized representation of the conjugates in their simplest forms. Possibly, some of the $TPPF_{20}$ porphyrins may be attached to the MNPs by more than one pentafluorophenyl group. The formation of the nanoplatforms ($MNPSiNH_2$) was done following the procedure described in a previous work.[10] Subsequently, $TPPF_{20}$ was selected as a porphyrin derivative with good versatility that allows the modifications of its functional groups with simple synthetic procedures. With a A_4 symmetry, this porphyrin is decorated with four pentafluorophenyl group. The synthetic versatility relies on the fluorine atom at the *para* position, which is prone to undergo S_NAr by different nucleofiles.[22,31] The reaction of pentafluorophenyl substituents in the porphyrin macrocycle to the amine groups of MNPs was previously described.[8,9] To synthesize MNP-P1, $MNPSiNH_2$ was mixed with an excess of $TPPF_{20}$. The coupling reaction was done in DMF stirring for 48 h at room temperature. MNP-P1 is a versatile nanoplatform that was used as starting material to obtain the other three conjugates. First, the porphyrin structure in this conjugate was modified to obtain MNP-P2. For a successful reaction, the following stoichiometric ratio was necessary (with respect to the concentration of $TPPF_{20}$ in MNP-P1): $TPPF_{20}$ 1 equiv., DAE 20 equiv. and KOH 16 equiv. Due to $TPPF_{20}$ bound to MNP has three substitutable groups, the previous stoichiometric triplicates. For this purpose, MNP-P1 was reacted with DAE in basic conditions using TBAB as a catalyst. After 12 h at room temperature the photosensitizing nanomagnet containing dimethylaminoethoxy ramifications was obtained (MNP-P2). This modification provides to each porphyrin unit of basic amine groups, which can acquire positive charges by protonation in a biological medium.[28,32] These ramifications can improve the MNPs binding to the microbial cell wall. It is known that the great majority of pathogens have an overall negative charge on the external wall.[7] With this under consideration, cationic analogues of MNP-P1 and MNP-P2 were synthesized. In the case of MNP-P1, the primary amine groups attached

to the MNPs were exhaustively methylated with an excess of methyl iodide to obtain MNP^{+}-P1. Similarly, primary and tertiary amines in MNP-P2 were precursors of positive charges to form MNP^{+}-$P2^{+}$. Through this reaction both, the free aminopropyl groups on the core of the Fe_3O_4 MNPs and the dimethylaminoethoxy substituents attached to the porphyrin were positively charged. Thus, both conjugates are surrounded by intrinsic positive charges. In particular, in the MNP^{+}-$P2^{+}$ the cationic centers are isolated from the porphyrin ring by an aliphatic spacer, which provides a higher mobility of the charge facilitating the interaction with the cell envelope. To remark on these synthetic pathways based on a nanoplatform concept is that in all cases the conjugates were easily purified by magnetic decantation and the MNPs were recovered in > 95% yields.

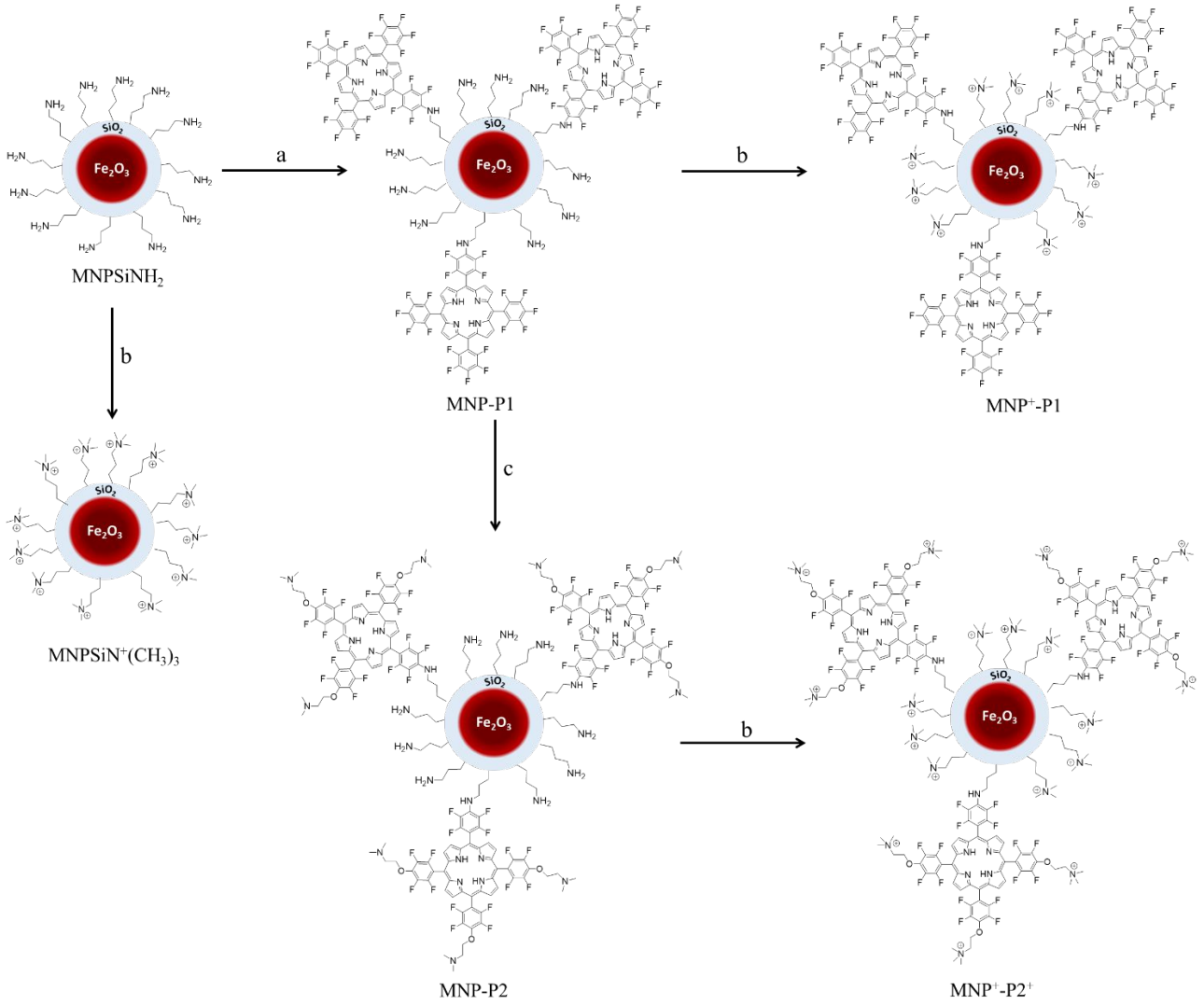

Figure 1. Simplified structures of the MNPs synthesized in this work. Reagents and conditions: a) $TPPF_{20}$, DMF, r.t., 48 h; b) CH_3I, DMF, 40 °C, 72 h; c) DAE, THF, KOH, TBAB, r.t., 12 h.

3.2. Characterization of conjugates by TEM and zeta potential

TEM images reveled that the average size of the MNPs in all conjugates was 12 ± 2 nm (Figure S2). Particles with similar sizes were previously obtained using a similar synthetic procedure.[10] The coating of the MNPs with $TPPF_{20}$ does not change the size of the particles. The images showed the formation of aggregates between MNPs due to the magnetization and attraction between the nanomagnet. Similar behavior was previously found for porphyrins attached to MNPs.[8,20]

On the other hand, the zeta potential (ζ) was determined to evaluate the surface load and stability of the suspensions. The values of ζ are indicated in Table 1. The ζ measurements yielded positive values in all conjugates. There is not a significant difference on the ζ values between the two control $MNPSiNH_2$, $MNPSiN^+(CH_3)_3$ as expected due to protonation of the amine at pH ~7. However, the ζ value dropped from 28 mV to 16 mV and from 25 to 19 mV upon covalently binding $TPPF_{20}$ to $MNPSiNH_2$ and $MNPSiN^+(CH_3)_3$, respectively. The difference in these values may be due to the fact that the bulky neutral porphyrin groups on the external layer of the MNPs produce a decrease in the overall surface charge, decreasing the amount of exposed cationic amines. However, ζ values increased 11 mV and 14 mV upon decorating MNP-P1 and MNP^+-P1 with tertiary amines to yield MNP-P2 and MNP^+-$P2^+$, respectively. These increase in ζ values with the amount of positive charges is expected for this kind of aggregates, as it was previously described.[33,34] An overall analysis of the colloidal stability and in accordance to the electrostatic interactions of the conjugates, the order is the following: MNP^+-$P2^+$ > MNP-P2 > MNP^+-P1 ~ MNP-P1. An increasing on the amount of positive charges enhances MNPs repulsion and favors the stability.

3.3. Absorption and fluorescence spectroscopic properties of conjugates

The UV-visible absorption spectra of MNPs conjugates are shown in Figure 2A. Furthermore, they are compared with those of MNPSiNH2 and a water-soluble porphyrin $TPPS^{4-}$, which was used as a reference. Spectra of MNPs conjugates were corrected considering the scattering of the $MNPSiNH_2$ (Figure 2A, inset). Suspensions of these conjugates in water showed the typical porphyrin Soret band at ~430 nm (Table 1). Also, the four Q-bands can be observed between 515 and 650 nm of the modified $TPPF_{20}$ attached to the MNPs. Therefore, absorption spectra also confirmed the binding of $TPPF_{20}$ to MNPs. Moreover, the absorption spectra of conjugates were carried out in DMF (Figure S3). Similar to those obtained in water, well defined bands of porphyrin are observed in this organic solvent and thus, they can be compared with that of $TPPF_{20}$. Upon attachment of $TPPF_{20}$ and its consecutive analogues to the MNPs, a ~20 nm bathochromic shift in the *Soret* band was observed in all the conjugates. This displacement of the band to higher wavelength can be attributed to immobilization of the porphyrin core to the MNPs with different electronic properties. This effect was also visualized in similar systems when a porphyrin is anchored to MNPs.[10,35]

The fluorescence emission spectra of the conjugates and $TPPS^{4-}$ in water are given in Figure 2B. Porphyrin unit attached to MNPs presented two bands in the four conjugates centered at 657 and 713 nm, which are characteristic of free-base porphyrin derivatives (Table 1). These emission bands correspond to Qx(0-0) and Qx(0–1) transitions.[11,36] The spectrum of porphyrin bound to MNPs in water maintains the shape of $TPPF_{20}$ in DMF, with the band at higher wavelength more intense than the first.[36] The presence of the MNPs was also reflected on a 20 nm shift to lower energy compare to $TPPF_{20}$ alone in DMF. Furthermore, a Stokes shifts of ~5 nm were calculated for the conjugates taken into account the intersection of the absorption and fluorescence spectra of the Qx(0-0) band in water. This small Stokes shifts indicate that in this porphyrin the spectroscopic energies are similar to the relaxed energies of the lowest singlet excited state, according to the rigid planar structure of the tetrapyrrolic macrocycle. Therefore, only a minor geometric relaxation occurs in the first excited state of $TPPF_{20}$ attached to MNPs. Fluorescence quantum yields (Φ_F) of these conjugates were calculated in water using $TPPS^{4-}$ as a reference (Table 1). The values of Φ_F for conjugates are smaller than that

of a free-base porphyrin in aqueous medium or $TPPF_{20}$ in DMF.[36] As it was previously shown, MNPs can quench emission from the singlet excited state of photosensitizers due to oxidative photoinduced electron transfer (PeT) from the porphyrin singlet excited state to the Fe_3O_4 nucleus.[20,37]

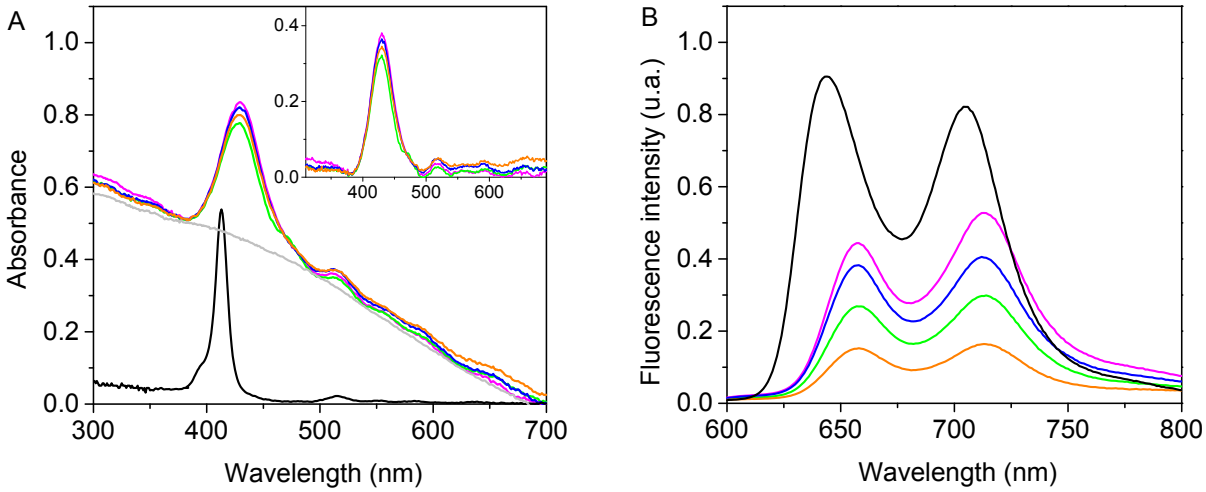

Figure 2. (A) UV-visible absorption spectra and (B) emission spectra of MNPs conjugates in water. MNP-P1 (magenta), MNP^{+}-P1 (green), MNP-P2 (blue), MNP^{+}-$P2^{+}$ (orange), $TPPS^{4-}$ (black) and $MNPSiNH_2$ scattering (gray). Inset: absorption spectra of the conjugates background corrected.

Table 1. Zeta potential (ζ) and spectroscopic properties of conjugates MNP-P1, MNP^{+}-P1, MNP-P2 and MNP^{+}-$P2^{+}$ in water.

Conjugates	ζ (mV) [a]	λ_{abs}^{Soret} (nm)	λ_{em}^{max} (nm)	Φ_F [b]
MNP-P1	16	430	657	0.036±0.003
MNP^{+}-P1	19	430	657	0.021±0.002
MNP-P2	27	430	657	0.028±0.003
MNP^{+}-$P2^{+}$	33	429	657	0.011±0.001

[a] ζ = 28 mV for $MNPSiNH_2$ and ζ = 25 mV for $MNPSiN^{+}(CH_3)_3$; [b] fluorescence quantum yields using $TPPS^{4-}$ as the reference $\Phi_F = 0.080$ in water.[25]

3.4. Photosensitized oxidation of substrates

The formation of $O_2(^1\Delta_g)$ sensitized by conjugates in water was detected by the decomposition of ABMM to form the corresponding 9,10-endoperoxide product ABMM-O_2.[27] Despite the short lifetime of $O_2(^1\Delta_g)$ in water (~4 μs), ABMM can act as effective trapping probe of this ROS due to its high solubility in aqueous solutions. Photooxidation of ABMM induced by conjugates was compared with that photosensitized by an anionic water-soluble porphyrin $TPPS^{4-}$. Figure 3A describes the progress of the decomposition reaction for ABMM as first-order kinetic plots. From these plots, the values of k_{obs}^{ABMM} were calculated and they are given in Table 2. Photooxidation of ABMM was not observed in presence of $MNPSiN^+(CH_3)_3$ (Figure 3A). The photodecomposition rate of the ABMM sensitized by conjugates was about six times higher than that found for $TPPS^{4-}$ in water. Moreover, highest values of k_{obs}^{ABMM} were obtained with MNP^+-P1 and MNP^+-$P2^+$, in comparison with those produced by MNP-P1 and MNP-P2. Similar results were also found when the ABMM decomposition was studied in PBS (Figure S4, Table 2). These can be attributed to the presence of four anionic groups on the malonic groups of ABMM.[27] These negative charges are involved in electrostatic interactions with the positively charged of MNPs. Thus, the ABMM are located close to the side where the is sensitized by $TPPF_{20}$, producing an increase in the decomposition rate of ABMM. This effect was more pronounced in conjugated with intrinsic cationic charges. In contrast, the anionic photosensitizer $TPPS^{4-}$ was repelled by the negative charges of ABMM.

To avoid this electrostatic interaction, the production of $O_2(^1\Delta_g)$ by the conjugates was evaluated monitoring the decomposition of DMA in DMF under aerobic condition (Figure 3B).[20] The values of k_{obs}^{DMA} were calculated from first-order kinetic plots of the DMA absorption at 378 nm with time. Negligible decomposition of DMA was found using $MNPSiN^+(CH_3)_3$ (Figure 3B). As can be observed in Table 2, similar reaction rates were found for the conjugates, although slightly higher for MNP-P1 and MNP^+-P1. However, the k_{obs}^{DMA} values sensitized by conjugates are less than half than

that found for $TPPS^{4-}$ in this organic solvent. Similar result was also observed for the decomposition of DMA sensitized by $TPPF_{20}$. From the kinetic data of DMA decomposition, the values of Φ_Δ were calculated by comparing the reaction rates for the conjugates with that for the reference ($TPPS^{4-}$).[11] Comparable values can be also obtained using $TPPF_{20}$ as a reference ($\Phi_\Delta = 0.70$).[38] The results for Φ_Δ are summarized in Table 2. On average, the Φ_Δ for all the conjugates was 0.25 being the highest value for MNP-P1 (0.34) and the lowest for MNP-P2 (0.17). Values of Φ_Δ of the same magnitude were previously found for porphyrin attached to MNPs.[10] Comparing these values to the reference (Table 2), it can be noticed that the presence of the supermagnetic core in close proximity of the porphyrin ring affects the triplet excited state of the photosensitizer, which is responsible for producing the cytotoxic species. As described above, magnetite quenches the fluorescence emission of porphyrin units bound to MNPs possibly by PeT.[37] This process can compete with the intersystem crossing producing a decrease triplet state formation and consequently $O_2(^1\Delta_g)$ production.[20] Furthermore, the partial aggregation of the immobilized porphyrin molecules in the MNP can preclude the photodynamic activity.[10] Likewise, the photodynamic activity to produce $O_2(^1\Delta_g)$ sensitized by conjugates was high enough to induce damage in microbial cells.

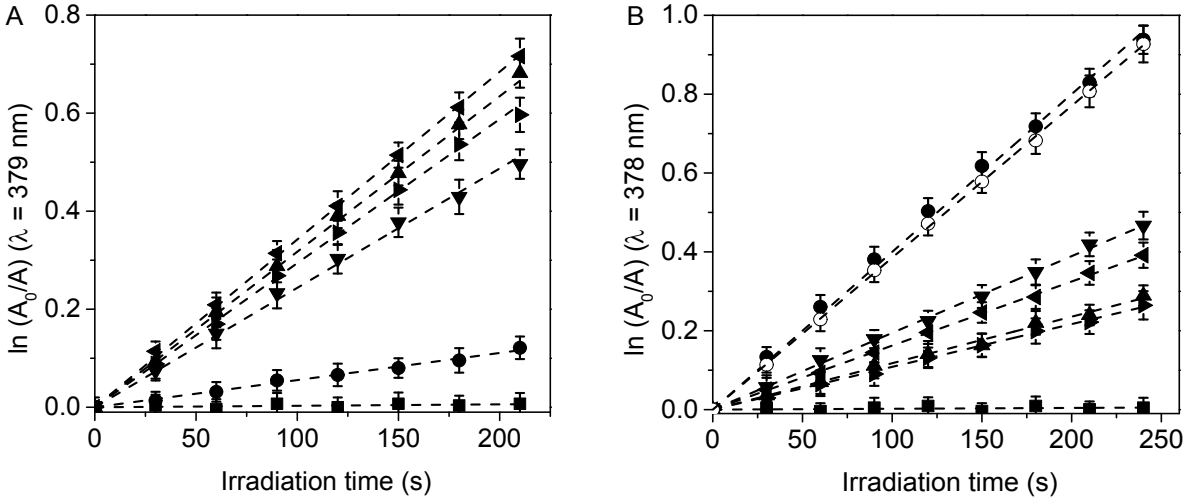

Figure 3. First-order plots for the photooxidation of (A) ABMM (35 μM) in deionized water and (B) DMA (35 μM) in DMF photosensitized by MNP-P1 (▼), MNP^+-P1 (◀), MNP-P2 (▶), MNP^+-$P2^+$ (▲), $MNPSiN^+(CH_3)_3$ (■), $TPPS^{-4}$ (●) and $TPPF_{20}$ (○); λ_{irr}= 455-800 nm.

Table 2. Kinetic parameters for the photooxidation reaction of ABMM (k_{obs}^{ABMM}), DMA (k_{obs}^{DMA}), Trp (k_{obs}^{Trp}), and singlet molecular oxygen quantum yield (Φ_Δ) sensitized by conjugates MNP-P1, MNP^+-P1, MNP-P2 and MNP^+-$P2^+$.

Conjugates	k_{obs}^{ABMM} (s^{-1}) [a]	k_{obs}^{ABMM} (s^{-1}) [b]	k_{obs}^{DMA} (s^{-1}) [c]	Φ_Δ [d]
MNP-P1	(2.4±0.1)x10^{-3}	(1.9±0.1)x10^{-3}	(1.9±0.1)x10^{-3}	0.34±0.02
MNP^+-P1	(3.4±0.3)x10^{-3}	(2.9±0.2)x10^{-3}	(1.6±0.1)x10^{-3}	0.29±0.02
MNP-P2	(2.9±0.2)x10^{-3}	(1.9±0.1)x10^{-3}	(1.0±0.1)x10^{-3}	0.17±0.01
MNP^+-$P2^+$	(3.2±0.2)x10^{-3}	(3.1±0.2)x10^{-3}	(1.2±0.1)x10^{-3}	0.21±0.01
$TPPS^{4-}$	(5.5±0.3)x10^{-4}	(7.8±0.4)x10^{-4}	(4.0±0.4)x10^{-3}	0.71

[a] In water; [b] in PBS; [c] in DMF, k_{obs}^{DMA} = 3.9x10^{-3} s^{-1} using $TPPF_{20}$ as a photosensitizer; [d] in DMF using $TPPS^{4-}$ as the reference.

3.5. PDI in cell suspensions

For the PDI experiments we selected two bacterial strain and a yeast with the intention of testing the conjugates *in vitro* in pathogenic microorganism with different cell envelopes complexities.[7] Suspensions of the Gram-positive *S. aureus*, the Gram-negative *E. coli* and the yeast *C. albicans* were treated with 0.2 mg MNPs conjugate/mL (2 μM immobilized $TPPF_{20}$) of the neutral and cationic conjugates. Control experiments showed that the viability of microbial cells was not affected by irradiation alone (Figure S5). Also, no toxicity was found in microorganisms treated with 0.2 mg/mL of the MNPs without porphyrin ($MNPSiNH_2$ and $MNPSiN^+(CH_3)_3$) and irradiated (Figure 4). Likewise, dark incubation with MNPs conjugates was not toxic to the cells. Therefore,

photokilling of microbial cells observed after irradiation of the cultures incubated with the MNPs conjugates was due to the photodynamic action sensitized by porphyrin.

Cell survival for cultures treated with conjugates are shown in Figure 4. Furthermore, photokilling capacities induced by conjugates were compared with those produced by the starting porphyrin. In all cases, the inactivation of the microbial cells treated with 2 μM $TPPF_{20}$ was less than that sensitized by the conjugates. Photoinactivation of microorganisms was dependent on irradiation times and conjugates. For all times irradiated, cell survival in the presence of the conjugates decreased significantly compared to control ($p < 0.05$). The photodynamic action sensitized by MNP^{+}-$P2^{+}$ produced 6 log decrease in *S. aureus* cell survival after 30 min irradiation (Figure 4A). Similar killing activity was found for MNP^{+}-P1 and MNP-P2 ($p > 0.05$), reaching 4 log of cell inactivation, while MNP-P1 induced 3.5 log reduction in cell viability. Also, MNP^{+}-$P2^{+}$ was effective to inactivate *S. aureus* at shorter irradiation time of 15 min, producing 5 log of killing. Furthermore, *E. coli* suspensions treated with MNP^{+}-$P2^{+}$ and irradiated for 15 min produced 2.7 log decrease in viability, whereas the photosensitizing activity of this conjugate exhibited 4.5 log units after 30 min (Figure 4B). In the Gram-negative bacteria, lowest inactivating effect was also found for MNP-P1, producing a reduction of 2 log. In addition, photokilling activity induced by MNP^{+}-P1 was slightly more effective than MNP-P2. Moreover, the photodynamic effect sensitized by the conjugates was compared in the yeast *C. albicans* (Figure 4C). After PDI treatment for 30 min, photoinactivation of cultures incubated with MNP^{+}-$P2^{+}$ yielded 3.7 log decrease in the cell viability. Photokilling of 2.8 log and 2.4 log were found for MNP^{+}-P1 and MNP-P2, respectively. In contrast, photocytotoxic effect mediated by MNP-P1 produced 1.9 log reduction in the survival of the yeast cells.

Comparing the inactivation in both prokaryote cells, the Gram-positive was more susceptible than the Gram-negative to the photodynamic effect induced by conjugates. This difference between the two types of bacteria can be understood by considering the structural characteristics of the cell envelope. Gram-positive bacteria have a cell wall composed of lipoteichoic and teichoic acids, which are organized in multiple layers of peptidoglycan.[39] This cellular envelope gives permeability to the

bacteria wall to facilitate the anchoring and the photodynamic action of the PSs.[7] In contrast, Gram-negative bacteria have a complex outer membrane on the cell wall, which contains phospholipids, lipopolysaccharides, lipoteichoic acids, and lipoproteins, producing a protective barrier impervious to antimicrobial agents. The constituents of the Gram-negative cell wall generate electrostatic interactions with cationic PSs that promote destabilization of the native organization of the cell envelope. In the case of yeast, this eukaryotic cell contains a wall with chitin, glucans and lipoproteins that represent a barrier with intermediate permeability in comparison to Gram-positive and Gram-negative bacteria.

It is not easy to compare the PDI results obtained here with previous investigations due to the different experimental conditions used. In was demonstrated that 5,10,15-tris(1-methylpyridinium-4-yl)-20-(pentafluorophenyl)porphyrin immobilized in cationized silica-coated MNPs of Fe_3O_4 was effective in the photoinactivation of both Gram-positive and Gram-negative bacteria.[8] Also, the analogue with a $CoFe_2O_4$ core showed a notable antimicrobial activity using water contaminated with the Gram-negative bacterium *Allivibrio fischeri*.[9] Furthermore, a cationic indium phthalocyanine attached to MNPs of Fe_3O_4 showed to be effective in the photoinactivation of *E. coli*.[40] The log reduction produced by this material was greater than the accepted log 3 and it can be easily separated with a magnet. Also, a ClIn(III) octacarboxy phthalocyanine bound to MNPs were investigated to reduce *S. aureus* cells in water samples.[41] This MNPs provided 90.6% photokilling of microbes in a water sample from the stream. In the same way, a cationic indium porphyrin conjugated to $Ag/CuFe_2O_4$ nanoparticles were able to photosensitize the inactivation of *S. aureus*.[42] The quaternized porphyrin attached to $Ag/CuFe_2O_4$ MNPs produced a high reduction in the S. aureus cell survival. A multifunctional chitosan functionalized magnetic chlorin e6 was constructed to combat *S. aureus* infection, showing an effective *in vitro* photodynamic sterilization ability.[43] Target-oriented photofunctional nanoparticles were fabricated by an esterification reaction to introduce hematoporphyrin and *S. aureus* antibody to the surface of Fe_3O_4 nanoparticles.[44] The results *in vitro* showed that these MNPs killed selectively *S. aureus* in L-929 cells and the PDI effect was also

confirmed *in vivo* experiments. Moreover, a nanosystem for early sepsis diagnosis and complete extracorporeal blood disinfection was prepared based on Fe_3O_4 nanoparticles functionalized with chlorin e6 and bacterial species-identifiable aptamers.[45] This nanosystem was used for successful diagnosis of sepsis caused by single *S. aureus* or multiple *S. aureus* and *E. coli* species of bacteria in mice. Under conditions similar to those used in the present study, PDI was investigated using 5,10,15,20-tetrakis(4-carboxyphenyl)porphyrin covalently bound to $MNPSiNH_2$.[10] The photodynamic effect of this MNPs produced 2.5 log reduction in *S. aureus* and *C. albicans*, while the decrease reached 3 log in *E. coli*, after 30 min irradiation. In the present investigation, MNP^+-$P2^+$ showed outstanding results, inactivating 99.9999% of the *S. aureus* strain in 30 min followed by 99.99% and 99.98% annihilation of *E. coli* and *C. albicans*, respectively. Therefore, this is an interesting photosensitizing conjugate to eradicate microorganisms.

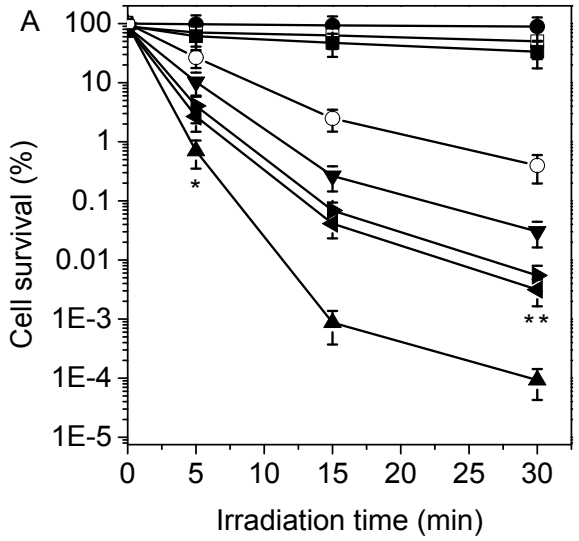

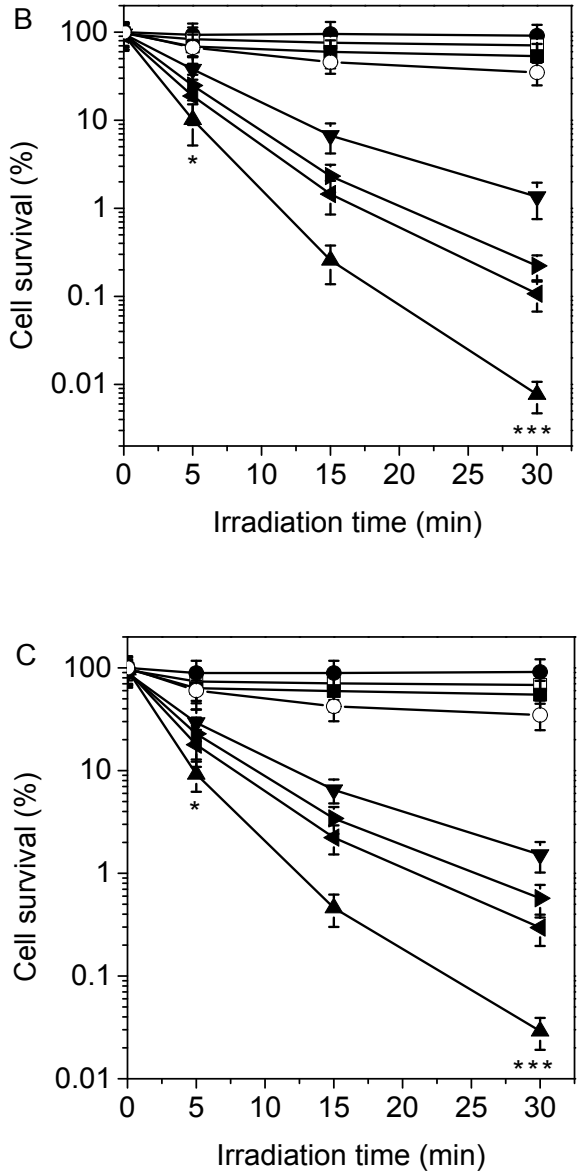

Figure 4. Cells survival of (A) *S. aureus*, (B) *E. coli* and (C) *C. albicans* cell suspensions treated with MNP-P1 (▼), MNP^+-P1 (◀), MNP-P2 (▶), MNP^+-$P2^+$ (▲) (0.2 mg MNPs conjugate/mL, 2 μM immobilized $TPPF_{20}$) and $TPPF_{20}$ (○) (2 μM) for 30 min at 37 ºC in dark and exposed to irradiation with visible light (90 mW/cm^2) for different times. Controls of untreated cells (●), cells incubated with $MNPSiNH_2$ (□) and $MNPSiN^+(CH_3)_3$ (■) (* $p < 0.05$ compared with control, ** $p > 0.05$ compared between MNP^+-P1 and MNP-P2, *** $p < 0.05$ compared between conjugates).

3.6. PDI recycling of MNP^+-$P2^+$

To test this concept, the recyclability of the MNP^{+}-$P2^{+}$ was assessed in cultures treated with MNP^{+}-$P2^{+}$. After incubation of the pathogens for 30 min in the dark, followed by exposition to visible light for 15 min (*S. aureus*) or 30 min (*E. coli* and *C. albicans*) the conjugate was recovered applying magnetic decantation and reused in another PDI cycle. Cell survival results after each cycle of PDI are shown in Figure 5. After a second cycle of PDI, the photokilling of the three microorganisms incubated with MNP^{+}-$P2^{+}$ was the same as in the first treatment. Furthermore, photoinactivation remained effective after a third cycle of PDI, there being no significant difference between the cell survival of the three PDI experiments. In this conjugate, the silica coating avoids the oxidation of magnetite and consequent degradation of the magnetic core. It was previously found that recycling was not possible using MNPs without the silica coating protection due to structural destruction and demagnetization.[10] In our case, the magnetic properties of the MNP^{+}-$P2^{+}$ allow the instant recovery of the conjugates after a treatment. Therefore, the PS attached to the MNPs can be reused several times. These experiments reveal that the porphyrin remains bound to the magnetic core with the same PDI potential over the cycles.

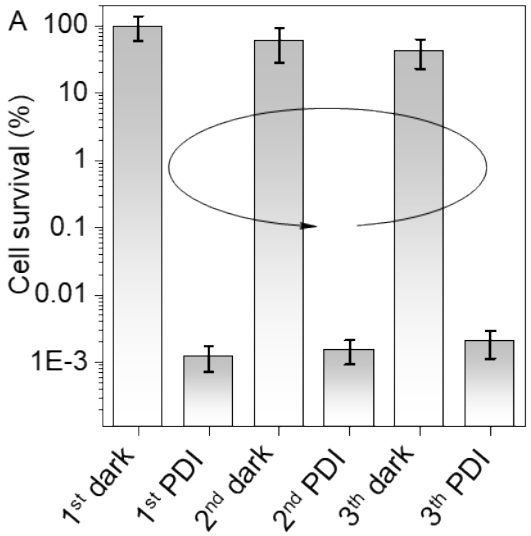

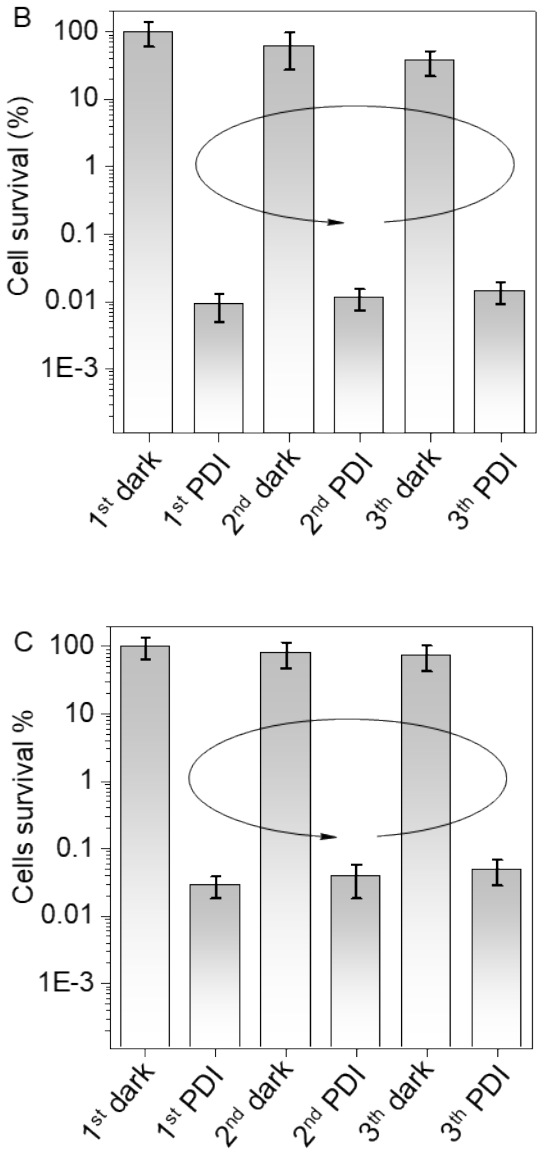

Figure 5. Cells survival of (A) *S. aureus*, (B) *E. coli* and (C) *C. albicans* treated with 0.2 mg MNPs conjugate/mL (2 μM immobilized $TPPF_{20}$) for 30 min in dark and exposed to irradiation with visible light (90 mW/cm^2) for 15 min (*S. aureus*) and 30 min (*E. coli* and *C. albicans*).

3.7. Binding and PDI of MNP^+-$P2^+$ by fluorescence microscopy

In the subsequent set of experiments, we examined cell binding and PDI efficacy of MNP^+-$P2^+$ by observing bacteria under a fluorescence microscope. To focus on a determinate number of bacteria, we used a technique previously describe that involves monitoring cells attached to the surface of a coverslip in a chamber containing 200 μL of PBS.[30] This experimental approach relies on bacterial pilus; protrusions that assist bacterial attachment on a surface. Unfortunately, *C. albicans*

lacks of these protrusions, reason why the yeast was left aside for this assay. Each fluorescence image was accompanied with a phase contrast photograph to confirm the presence and position of the bacteria. After incubation of the cells with 0.8 mg MNP^{+}-$P2^{+}$ in 200 mL PBS for 30 min in dark, florescence intensity reached a plateau for either *S. aureus* and *E. coli*, indicating complete cellular uptake of conjugate (Figure 6, first row). As can be observed, the red emission of MNP^{+}-$P2^{+}$ was detected for both bacteria, indicating the binding of this conjugate to the cells. After a previous incubation with MNP^{+}-$P2^{+}$ for 30 min in the dark, PI was added and the cells were incubated for another 15 min. PI is a well-known cell death marker that bind to DNA by intercalating between the bases upon membrane disruption.[46] Unbound PI has a Φ_F ~0.01, similar to the value obtained for MNP^{+}-$P2^{+}$ in aqueous medium. Upon PI binding to DNA this emission value can increase up to 30-fold.[47] Since the emission spectrum of MNP^{+}-$P2^{+}$ and the PI overlaps, we used this difference in the values of the Φ_F to distinguish between dead cells and living cells. Basically, the sensibility in the CMOS camera was lowered down until no fluorescence was observed after preincubation of bacteria with the PS, using a light dose of 1.2 J/cm^2. After 30 min of PDI therapy all bacteria of either strain were dead showing the enhanced red fluorescence from the cell death marker (Figure 6, middle row). Moreover, control experiments with MNP^{+}-P^{2+} and PI incubated for 75 min (30 min to ensure PS uptake, 15min to ensure PI uptake if cells are initially dead and another 30 min as control) but no irradiation showed negligible red fluorescence emission, indicating that pathogens inactivation occurs only in the presences of light (Figure 6, last row). These experiments demonstrate that the MNP^{+}-P^{2+} conjugate was also effective in photoinactivating bacteria attached to a surface, an oversimplified example of a first stage of biofilm formation.

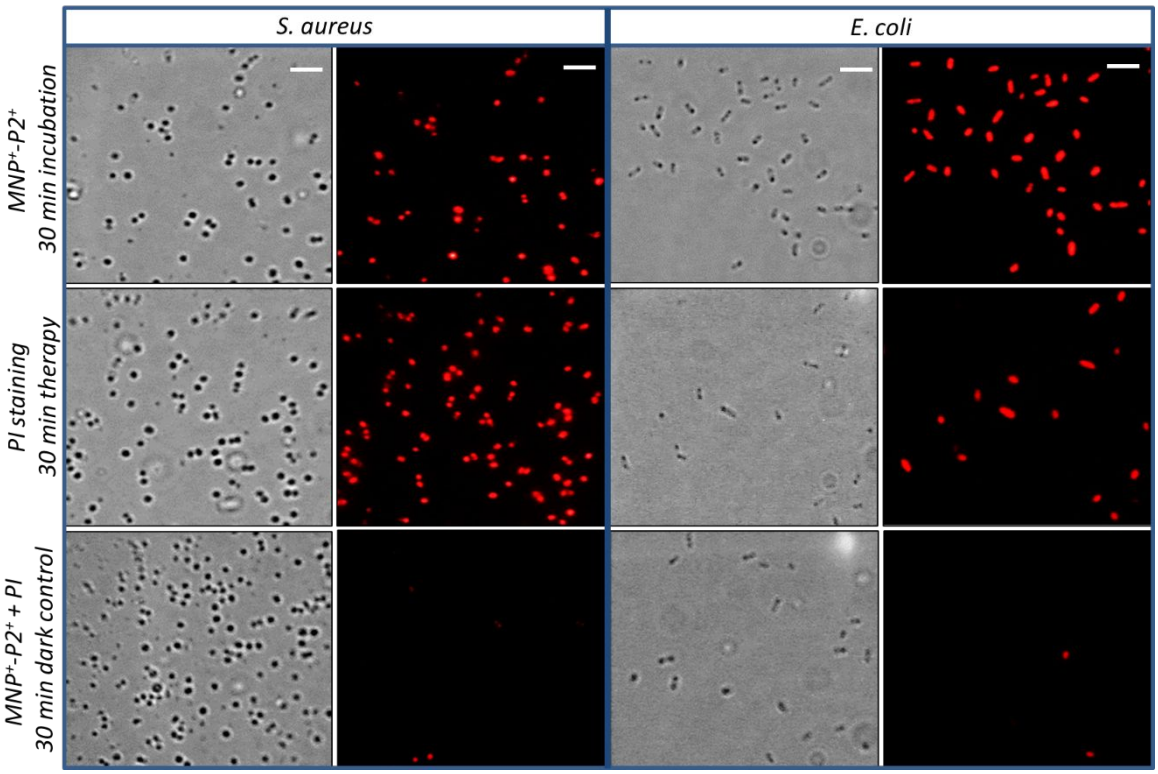

Figure 6. Microscopic images of *S. aureus* and *E. coli* incubated with 0.2 mg MNPs conjugate/mL (2 μM immobilized $TPPF_{20}$) for 30 min in the dark and then irradiated with visible light for 30 min. First and third columns, cells under bright field; second and fourth columns, fluorescence emission fluorescence emission of PI after the PDI treatment (scale bar 5 μm).

4. CONCLUSIONS

In this work, the MNP-P1 conjugate was synthesized by covalently binding $TPPF_{20}$ to MNPSiNH2 through the S_NAr reaction of the F atom in the *para* position of the pentafluorophenyl groups of the porphyrin. This conjugate was the platform to obtain modifications in the tetrapyrrolic macrocycle. Thus, it was possible to add dimethylaminoethoxy groups to the $TPPF_{20}$ porphyrin immobilized on the MNPs. This synthetic modification also involves the S_NAr reaction of the F atoms in the *para*-remaining positions to produce MNP-P2. The periphery of this conjugate is crowded with basic aliphatic amine groups, which can acquire positive charges in aqueous media by protonation.

Furthermore, the amine substituents in MNP-P1 and MNP-P2 were methylated to form conjugates with intrinsic cationic charges named MNP^+-P1 and MNP^+-$P2^+$, respectively. An average size of 12

± 2 nm was found for these MNPs, while the main difference between conjugates was the greater coating with positive charges of MNP^{+}-$P2^{+}$, as indicated by the ζ values. This approach of *in situ* modification and purification by magnetic decantation allows to obtain conjugates with a simple procedure and high yields. The UV-visible spectra of each conjugate showed the characteristic bands of the porphyrin that correspond to $TPPF_{20}$ immobilized in the MNPs. In all cases, a bathochromic shift of the Soret band was found with respect to it of free $TPPF_{20}$. Furthermore, the porphyrin bound to the MNPs retain the ability to emit red fluorescence. These spectroscopic results corroborated the binding between porphyrin and MNPs. On the other hand, the photodecomposition of oxidizable substrates in the presence of the different conjugates indicated an efficient production of $O_2(^1\Delta_g)$. PDI studies in *S. aureus*, *E. coli* and *C. albicans* indicate that MNP^{+}-$P2^{+}$ is the most effective conjugate for the eradication of microorganisms. In contrast, the lowest photoinactivating capacity was found for the unmodified MNP-P1 conjugate. Microscopic observations indicated the binding of MNP^{+}-$P2^{+}$ to cells and its ability to photoinactivate individual cells of bacteria attached to a surface. Moreover, this conjugate can be recycled and reused, reducing the costs of PDI applications and without contaminating the environment. Thus, *in situ* approach is a suitable scaffold to obtain modified conjugates and the intrinsically charged MNP^{+}-$P2^{+}$ is an interesting photoactive material to inactivate pathogens.

ASSOCIATED CONTENT

Supporting Information

The Supporting Information is available free of charge at https://pubs.acs.org/doi/.

Materials, instrumentation, methodology for the synthesis of conjugates, TEM images of conjugates, UV-visible absorption spectra of MNPs conjugates in DMF, First-order plots for the photooxidation of ABMM in PBS and cells survival controls of microorganisms (PDF).

AUTHOR INFORMATION

Corresponding Author

Edgardo N. Durantini − *Universidad Nacional de Río Cuarto, Río Cuarto, Argentina*; orcid.org/0000-0001-8901-7543; Phone: +54 358 4676157; E-mail: edurantini@exa.unrc.edu; Fax: +54 358 4676233

Other Authors

Ana C. Scanone − *Universidad Nacional de Río Cuarto, Río Cuarto, Argentina*; orcid.org/0000-0001-6306-216X

Natalia S. Gsponer − *Universidad Nacional de Río Cuarto, Río Cuarto, Argentina*; orcid.org/0000-0003-3012-7590

María G. Alvarez − *Universidad Nacional de Río Cuarto, Río Cuarto, Argentina*; orcid.org/0000-0002-1051-3390

Daniel A. Heredia − *Universidad Nacional de Río Cuarto, Río Cuarto, Argentina*; orcid.org/ 0000-0002-0667-3906

Andrés M. Durantini − *Universidad Nacional de Río Cuarto, Río Cuarto, Argentina*; orcid.org/ 0000-0002-7898-4033

Notes

The authors declare no competing financial interest.

ACKNOWLEDGEMENTS

Authors are grateful to ANPCYT (PICT-2016 0667), MINCyT Córdoba (PID-2018 36) and SECYT-UNRC (PPI-2020) for financial support. N.S.G, M.G.A., A.M.D, E.N.D. are Scientific Members of CONICET. A.C.S. thanks CONICET for a research fellowship.

REFERENCES

(1) Laurent, S.; Forge, D.; Port, M.; Roch, A.; Robic, C.; Elst, L. V.; Muller, R. N. Magnetic iron oxide nanoparticles: synthesis, stabilization, vectorization, physicochemical characterizations, and biological applications. *Chem. Rev.* **2008**, *108*, 2064-2110.

(2) Bañobre-López, M.; Teijeiro, A.; Rivas, J. Magnetic nanoparticle-based hyperthermia for cancer treatment. *Rep. Pract. Oncol. Radiother.* **2013**, *18*, 397-400.

(3) Li, Y.; Wang, N.; Huang, X.; Li, F.; Davis, T. P.; Qiao, R.; Ling, D. Polymer-assisted magnetic nanoparticle assemblies for biomedical applications, *ACS Appl. Bio Mater.* **2020**, *3*, 121-142.

(4) Zhou, K.; Zhou, X.; Liu, J.; Huang, Z. Application of magnetic nanoparticles in petroleum industry: a review. *J. Petrol. Sci. Eng.* **2020**, *188*, 106943.

(5) Mesquita, M. Q.; Dias, C. J.; Neves, M. G. P. M. S.; Almeida, A.; Faustino, M. A. F. Revisiting current photoactive materials for antimicrobial photodynamic therapy. *Molecules* **2018**, *23*, 2424.

(6) Feng, Y.; Liu, L.; Zhang, J.; Aslan, H.; Dong, M. Photoactive antimicrobial nanomaterials. *J. Mater. Chem. B* **2017**, *5*, 8631-8652.

(7) Durantini, A. M.; Heredia, D. A.; Durantini, J. E.; Durantini, E. N. BODIPYs to the rescue: potential applications in photodynamic inactivation. *Eur. J. Med. Chem.* **2018**, *144*, 651-661.

(8) Carvalho, C. M. B.; Alves, E.; Costa, L.; Tomé, J. P. C.; Faustino, M. A. F.; Neves, M. G. P. M. S.; Tomé, A. C.; Cavaleiro, J. A. S.; Almeida, A.; Cunha, A.; Lin, Z.; Rocha, J. Functional cationic nanomagnet-porphyrin hybrids for the photoinactivation of microorganisms. *ACS Nano* **2010**, *4*, 7133-7140.

(9) Alves, E.; Rodrigues, J. M. M.; Faustino, M. A. F.; Neves, M. G. P. M. S.; Cavaleiro, J. A. S.; Lin, Z.; Cunha, Â.; Nadais, M. H.; Tomé, J. P. C.; Almeida, A. A new insight on nanomagneteporphyrin hybrids for photodynamic inactivation of microorganisms. *Dyes Pigm.* **2014**, *110*, 80-88.

(10) Scanone, A. C.; Gsponer, N. S.; Alvarez, M. G.; Durantini, E. N. Photodynamic properties and photoinactivation of microorganisms mediated by 5,10,15,20-tetrakis(4-

carboxyphenyl)porphyrin covalently linked to silica-coated magnetite nanoparticles. *J. Photochem. Photobiol. A: Chem.* **2017**, *346*, 452-461.

(11) Scanone, A. C.; Gsponer, N. S.; Alvarez, M. G.; Durantini, E. N. Porphyrins containing basic aliphatic amino groups as potential broad-spectrum antimicrobial agents. *Photodiagn. Photodyn. Ther.* **2018**, *24*, 220-227.

(12) Durantini, E. N.; Silber, J. J. Synthesis of 5-(4-acetamidophenyl)-10,15,20-tris(4-substituted phenyl) porphyrins using dipyrromethanes. *Synth. Commun.* **1999**, *29*, 3353-3368.

(13) Ballatore, M. B.; Spesia, M. B.; Milanesio, M. E.; Durantini, E. N. Synthesis, spectroscopic properties and photodynamic activity of porphyrin-fullerene C_{60} dyads with application in the photodynamic inactivation of Staphylococcus aureus. *Eur. J. Med. Chem.* **2014**, *83*, 685-694.

(14) Dommaschk, M.; Gutzeit, F.; Boretius, S.; Haag, R.; Herges, R. Coordination-induced spin-state-switch (CISSS) in water. *Chem. Commun.* **2014**, *50*, 12476-12478.

(15) Heredia, D. A.; Martínez, S. R.; Durantini, A. M.; Pérez, M. E.; Mangione, M. I.; Durantini, J. E.; Gervaldo, M. A.; Otero, L. A.; Durantini, E. N. Antimicrobial photodynamic polymeric films bearing biscarbazol triphenylamine end-capped dendrimeric Zn(II) porphyrin. *ACS Appl. Mater. Interfaces* **2019**, *11*, 27574-27587.

(16) Bhupathiraju, N. V. S. D. K.; Rizvi, W.; Batteas, J. D.; Drain, C. M. Fluorinated porphyrinoids as efficient platforms for new photonic materials, sensors, and therapeutics. *Org. Biomol. Chem.* **2016**, *14*, 389-408.

(17) Olofsson, M.; Matussek, A.; Ehricht, R.; Lindgren, P. E.; Östgren, C. J. Differences in molecular epidemiology of *Staphylococcus aureus* and *Escherichia coli* in nursing home residents and people in unassisted living situations. *J. Hosp. Infect.* **2019**, *101*, 76-83.

(18) Singh, R.; Singh, A. P.; Kumar, S.; Giri, B. S.; Kim, K. H. Antibiotic resistance in major rivers in the world: a systematic review on occurrence, emergence, and management strategies. *J. Clean. Prod.* **2019**, *234*, 1484-1505.

(19) Janbon, G.; Quintin, J.; Lanternier, F.; d'Enfert, C. Studying fungal pathogens of humans and fungal infections: fungal diversity and diversity of approaches. *Microb. Infect.* **2019**, *21*, 6237-6245.

(20) Scanone, A. C.; Santamarina, S. C.; Heredia, D. A.; Durantini, E. N.; Durantini, A. M. Functionalized magnetic nanoparticles with BODIPYs for bioimaging and antimicrobial therapy applications. *ACS Appl. Bio Mater.* **2020**, *3*, 1061-1070.

(21) McClure, J. E.; Baudouin, L.; Mansuy, D.; Marzilli, L. G. Interactions of DNA with a new electron-deficient tentacle porphyrin: *meso*-tetrakis[2,3,5,6-tetrafluoro-4-(2-trimethylammoniumethylamine)phenyl]porphyrin. *Biopolymers* **1997**, *42*, 203-217.

(22) Gutsche, C. S.; Ortwerth, M.; Gräfe, S.; Flanagan, K. J.; Senge, M. O.; Reissig, H. U.; Kulak, N.; Wiehe, A. Nucleophilic aromatic substitution on pentafluorophenyl-substituted dipyrranes and tetrapyrroles as a route to multifunctionalized chromophores for potential application in photodynamic therapy. *Chem. Eur. J.* **2016**, *22*, 13953-13964.

(23) Golf, H. R. A.; Reissig, H-U.; Wiehe, A. Regioselective nucleophilic aromatic substitution reaction of *meso*-pentafluorophenyl-substituted porphyrinoids with alcohols. *Eur. J. Org. Chem.* **2015**, *7*, 1548-1568.

(24) Vasti, C.; Giacomelli, C. E.; Rojas, R. Pros and cons of coating layered double hydroxide nanoparticles with polyacrylate. Appl. Clay Sci. **2019**, *172*, 11-18.

(25) Kalyanasundaram, K.; Neumann-Spallart, M. Photophysical and redox properties of water-soluble porphyrins in aqueous media. *J. Phys. Chem.* **1982**, *86*, 5163-5169.

(26) Gottfried V., P. D., Winkelman J.W., Kimel S. Photosensitizers in organized media: singlet oxygen production and spectral properties. *Photochem. Photobiol.* **1988,** *48*, 157-163.

(27) Mora, S. J.; Milanesio, M. E.; Durantini, E. N. Spectroscopic and photodynamic properties of 5,10,15,20-tetrakis[4-(3-*N*,*N*-dimethylaminopropoxy)phenyl]porphyrin and its tetracationic derivative in different media. *J. Photochem. Photobiol. A: Chem.* **2013**, *270*, 75-84.

(28) Ferreyra, D. D.; Reynoso, E.; Cordero, P.; Spesia, M. B.; Alvarez, M. G.; Milanesio, M. E.; Durantini, E. N. Synthesis and properties of 5,10,15,20-tetrakis[4-(3-*N*,*N*-dimethylaminopropoxy)phenyl] chlorin as potential broad-spectrum antimicrobial photosensitizers. *J. Photochem. Photobiol. B: Biol.* **2016**, *158*, 243-251.

(29) Ballatore, M. B.; Milanesio, M. E.; Fujita, H.; Lindsey, J. S.; Durantini, E. N. Bacteriochlorin-bis(spermine) conjugate affords an effective photodynamic action to eradicate microorganisms. *J. Biophotonics* **2020**, *13*, e201960061.

(30) Martínez, S. R.; Palacios, Y. B.; Heredia, D. A.; Agazzi, M. L.; Durantini, A. M. Phenotypic resistance in photodynamic inactivation unravelled at the single bacterium level. *ACS Infect. Dis.* **2019**, *5*, 1624-1633.

(31) Vives, G.; Giansante, C.; Bofinger, R.; Raffy, G.; Del Guerzo, A.; Kauffmann, B.; Batat, P.; Jonusauskas, G.; McClenaghan, N. D. Facile functionalization of a fully fluorescent perfluorophenyl BODIPY: photostable thiol and amine conjugates. *Chem. Commun.* **2011**, *47*, 10425-10427.

(32) Quiroga, E. D.; Mora, S. J.; Alvarez, M. G.; Durantini, E. N. Photodynamic inactivation of *Candida albicans* by a tetracationic tentacle porphyrin and its analogue without intrinsic charges in presence of fluconazole. *Photodiag. Photodyn. Ther.* **2016**, *13*, 334-340.

(33) El-Shabouri, M.H. Positively charged nanoparticles for improving the oral bioavailability of cyclosporin-A. *Int. J. Pharm.* **2002**, *249*, 101-108.

(34) Reddy, P. M.; Chang, K. C.; Liu, Z. J.; Chen, C. T.; Ho, Y. P. Functionalized magnetic iron oxide (Fe_3O_4) nanoparticles for capturing Gram-positive and Gram-negative bacteria. *J. Biomed. Nanotech.* **2014**, *10*, 1429-1439.

(35) Penon, O.; Marín, M. J.; Amabilino, D. B.; Russell, D. A.; Pérez-García, L. Iron oxide nanoparticles functionalized with novel hydrophobic and hydrophilic porphyrins as potential agents for photodynamic therapy. *J. Colloid Interface Sci.* **2016**, *462*, 154-165.

(36) Heredia, D. A.; Durantini, A. M.; Sarotti, A. M.; Gsponer, N. S.; Ferreyra, D. D.; Bertolotti, S. G.; Milanesio, M. E.; Durantini, E. N. Proton-dependent switching of a novel amino chlorin

derivative as a fluorescent probe and photosensitizer for acidic media. *Chem. Eur. J.* **2018**, *24*, 5950-5961.

(37) Yu, C. J.; Wu, S. M.; Tseng, W. L. Magnetite nanoparticle-induced fluorescence quenching of adenosine triphosphate–BODIPY conjugates: application to adenosine triphosphate and pyrophosphate sensing. *Anal. Chem.* **2013**, *85*, 8559-8565.

(38) Grancho, J. C. P.; Pereira, M. M.; Miguel, M. da G.; Rocha Gonsalves, A. M.; Burrows, H. D. Synthesis, spectra and photophysics of some free base tetrafluoroalkyl and tetrafluoroaryl porphyrins with potential applications in imaging. *Photochem. Photobiol.* **2002**, *75*, 249-256.

(39) Malanovic, N.; Lohner, K. Gram-positive bacterial cell envelopes: the impact on the activity of antimicrobial peptides. *Biochim. Biophys. Acta-Biomembranes* **2016**, *1858*, 936-946.

(40) Osifeko, O. L.; Uddin, I.; Mashazi, P. N.; Nyokong, T. Physicochemical and antimicrobial photodynamic chemotherapy of unsymmetrical indium phthalocyanines alone or in the presence of magnetic nanoparticles. *New J. Chem.* **2016**, *40*, 2710-2721.

(41) Sindelo, A.; Nyokong, T. Magnetic nanoparticle-indium phthalocyanine conjugate embedded in electrospun fiber for photodynamic antimicrobial chemotherapy and photodegradation of methyl red. *Heliyon* **2019**, *5*, e02352.

(42) Makola, L. C.; Managa, M.; Nyokong, T. Enhancement of photodynamic antimicrobial therapy through the use of cationic indium porphyrin conjugated to $Ag/CuFe_2O_4$ nanoparticles. *Photodiagn. Photodyn. Ther.* **2020**, *30*, 101736.

(43) Lu, C.; Sun, F.; Liu, Y.; Xiao, Y.; Qiu, Y.; Mu, H.; Duan, J. Versatile Chlorin e6-based magnetic polydopamine nanoparticles for effectively capturing and killing MRSA. *Carbohydr. Polym.* **2019**, *218*, 289-298.

(44) Wang, K. K.; Shin, E. P.; Lee, H. J.; Jung, S. J.; Hwang, J. W.; Heo, I.; Kim, J. H.; Oh, M. K.; Kim Y. R. Target-oriented photofunctional nanoparticles (TOPFNs) for selective photodynamic inactivation of methicillin-resistant *Staphylococcus aureus* (MRSA). *J. Photochem. Photobiol. B: Biol.* **2018**, *183*, 184-190.

(45) Wang, J.; Wu, H.; Yang, Y.; Yan, R.; Zhao, Y.; Wang, Y.; Chen, A.; Shao, S.; Jiang, P.; Li, Y. Q. Bacterial species-identifiable magnetic nanosystems for early sepsis diagnosis and extracorporeal photodynamic blood disinfection. *Nanoscale* **2018**, *10*, 132-141.

(46) Duedu, K. O.; French, C. E. Two-colour fluorescence fluorimetric analysis for direct quantification of bacteria and its application in monitoring bacterial growth in cellulose degradation systems. *J. Microbiol. Methods* **2017**, *135*, 85-92.

(47) Samanta, A.; Paul, B. K.; Guchhait, N.; Photophysics of DNA staining dye propidium iodide encapsulated in bio-mimetic micelle and genomic fish sperm DNA. *J. Photochem. Photobiol. B: Biol.* **2012**, *109*, 58-67.

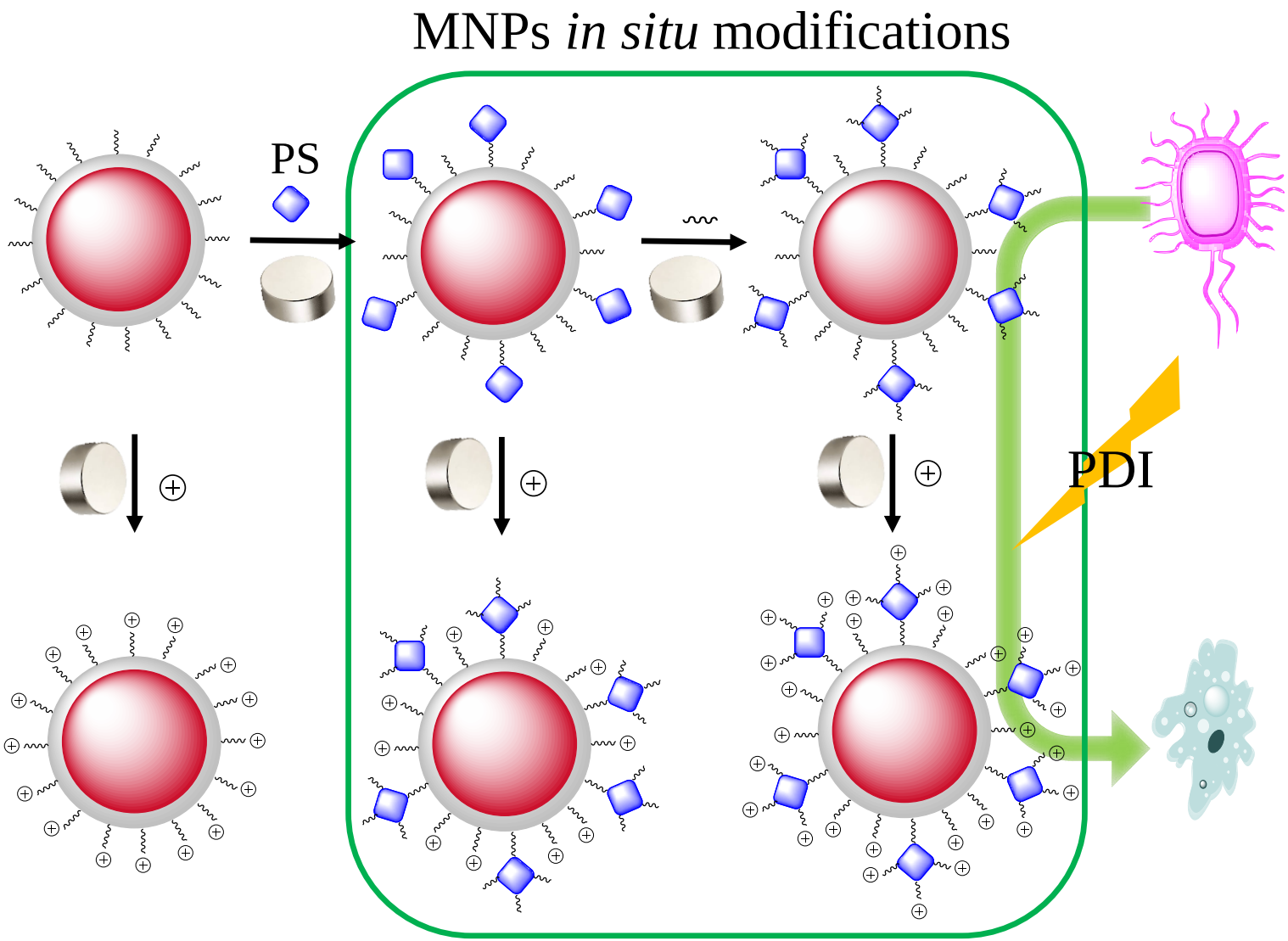
MNPs *in situ* modifications
PS
PDI